ARTICLE OPEN

Check for updates

Tuning the Fermi liquid crossover in Sr_2RuO_4 with uniaxial stress

A. Chronister[1]✉, M. Zingl[2], A. Pustogow[1,3], Yongkang Luo[1], D. A. Sokolov[4], F. Jerzembeck[4], N. Kikugawa[5], C. W. Hicks[4], J. Mravlje[6], E. D. Bauer[7], J. D. Thompson[7], A. P. Mackenzie[4,8], A. Georges[2,9,10,11] and S. E. Brown[1]✉

We perform nuclear magnetic resonance (NMR) measurements of the oxygen-17 Knight shifts for Sr_2RuO_4, while subjected to uniaxial stress applied along [100] direction. The resulting strain is associated with a strong variation of the temperature and magnetic field dependence of the inferred magnetic response. A quasiparticle description based on density-functional theory calculations, supplemented by many-body renormalizations, is found to reproduce our experimental results, and highlights the key role of a van-Hove singularity. The Fermi-liquid coherence scale is shown to be tunable by strain, and driven to low values as the associated Lifshitz transition is approached.

npj Quantum Materials (2022)7:113 ; https://doi.org/10.1038/s41535-022-00519-6

INTRODUCTION

Sr_2RuO_4 is widely recognized as the paradigmatic example of a very clean, strongly correlated Fermi liquid (FL) with a simple quasi-two-dimensional Fermi surface (FS), from which an unconventional superconducting ground state emerges[1,2]. While the superconducting state has been a subject of intense study[3–5], there are multiple attributes of Sr_2RuO_4 that motivate an in-depth analysis of the normal state, including the ability to characterize the FL state and quasiparticle dispersions with exquisite accuracy and the opportunity to study how the quasiparticles gradually lose coherence as temperature T is raised, evolving all the way into 'bad metal' behavior at high-T[6–8].

Indeed, FL behavior applies only below a characteristic crossover temperature $T_{FL} \sim 30$ K[9] and is characterized, among other properties, by the expected thermal variation of the resistivity $\delta\rho \sim T^2$ and an enhanced T-independent Pauli susceptibility[10,11]. Interestingly, before settling into the Fermi-liquid temperature independent susceptibility, the NMR signal displays a shallow maximum at about 40 K[11].

In the low-T FL regime, highly accurate determinations of the quasiparticle properties have been achieved using quantum oscillations (QO)[12,13], angle-resolved photoemission spectroscopy (ARPES)[14–16], and optical conductivity measurements[17]. The fermiology consists of three quasiparticle bands and associated FS sheets, conventionally labeled α, β, γ, forming predominantly from a hybridization of each of the Ru d_{xy}, $d_{zx,yz}$ orbitals with oxygen $2p$ orbitals. Spin–orbit coupling (SOC) affects the orbital character of the quasiparticles states and leads to a high degree of orbital mixing for the β and γ branches along the Brillouin Zone diagonal[16,18–21]. The gradual breakdown of the quasiparticle picture at higher temperatures is revealed by transport measurements (resistivity)[6] and Hall effect[22–24], as well as ARPES and optical spectroscopy[17].

The bands are strongly renormalized[13] by electronic correlations. Theoretical work suggested[7] that these correlations result from the combined effect of (i) the Hund's rule coupling[2,25], which has led to a characterization of Sr_2RuO_4 as a member of the broad family of 'Hund's metals' and (ii) importantly, the proximity of the Fermi level to a van-Hove singularity (vHs) associated with the quasi-2D γ band[8]. The effects of passing E_F through the vHs were experimentally studied with doping[15], straining of thin films[26] and application of uniaxial stress[27,28]. This last technique allows the effects of the vHs to be probed without introducing additional disorder. This was exploited also in a NMR study that revealed enhancements of the Knight shifts at the critical strain[25]. Theoretically, the study of the temperature dependence of the NMR response was reported[7] for the unstrained case, but the detailed response of the Fermi-liquid correlations to applied stress is still an open question. The ARPES results reported in refs. [15,26] found no evidence for increased mass enhancement near the vHs in the former, and only a weak enhancement in the latter. On the other hand, a significant increase of the T^2 coefficient associated with resistivity was reported under applied uniaxial stress[27]. This was later found to be consistent with a Boltzmann description of transport based on coherent quasiparticles close to a van-Hove singularity[29,30].

Here we address the role of the vHs by acquiring ^{17}O NMR data in the crucial temperature range around $T_{FL} \sim 30$ K, under conditions of variable uniaxial stress. The results provide direct evidence that the crossover scale T_{FL} is controlled by the location of the vHs relative to Fermi level E_F, and moreover that the associated singular DOS strongly influences the physical properties such as spin susceptibility over an extraordinarily broad temperature range. T_{FL} is driven to a vanishingly small value at the critical strain, and the spin susceptibility inferred from the ^{17}O Knight shift measurements exhibits the expected logarithmic temperature dependence for a two-dimensional vHs. The non-FL magnetic response at the critical strain is marked by a strong nonlinear field dependence[25], owing to comparable Zeeman and thermal energy scales, and a corresponding divergent singularity

[1]Department of Physics and Astronomy, UCLA, Los Angeles, CA 90095, USA. [2]Center for Computational Quantum Physics, Flatiron Institute, 162 5th Avenue, New York, NY 10010, USA. [3]Institute of Solid State Physics, TU Wien, 1040 Vienna, Austria. [4]Max Planck Institute for Chemical Physics of Solids, Dresden, Germany. [5]National Institute for Materials Science, Tsukuba 305-0003, Japan. [6]Jožef Stefan Institute, Jamova 39, 1000 Ljubljana, Slovenia. [7]Los Alamos National Laboratory, Los Alamos, NM, USA. [8]SUPA, School of Physics and Astronomy, University of St. Andrews, St. Andrews KY16 9SS, UK. [9]Collège de France, 11 Place Marcelin Berthelot, 75005 Paris, France. [10]Centre de Physique Théorique Ecole Polytechnique, CNRS, Université Paris-Saclay, 91128 Palaiseau, France. [11]DQMP, Université de Genève, 24 Quai Ernest Ansermet, 1211 Genève, Suisse.
✉email: aaronchronister@ucla.edu; brown@physics.ucla.edu

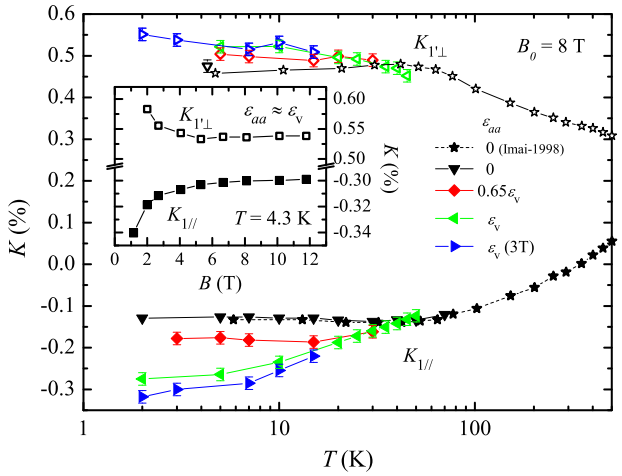

Fig. 1 Temperature-dependent ^{17}O NMR Knight shifts, for different fields and strains. ^{17}O shift measurements recorded under zero strain, critical strain, and an intermediate strain are shown in the main panel. Note that for the critical strain, the effects of the singularity are more substantial in $K_{1\|}$ than in $K_{1'\perp}$. Error bars are determined by the NMR linewidth. Inset: Shift vs field data from ref. [25]. The shifts at the critical strain ε_v exhibit a strong field dependence, observable for sufficiently low temperatures, that is associated with the Zeeman split of the singularity.

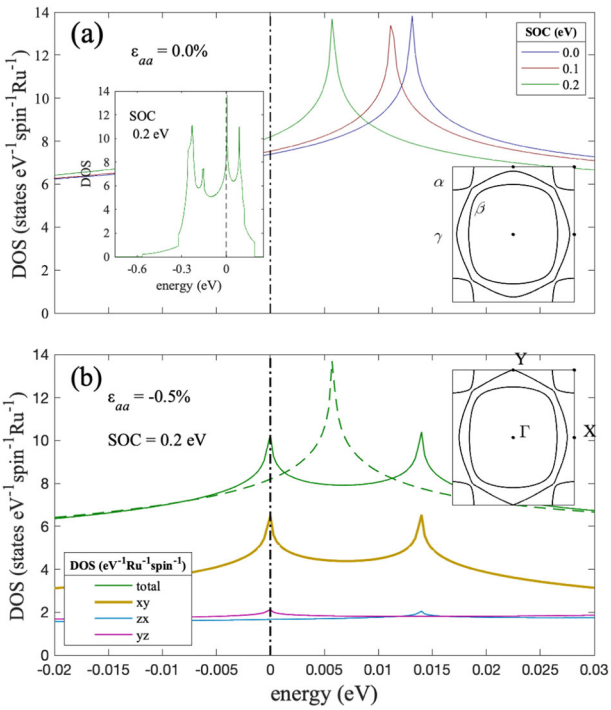

Fig. 2 Effect of strain and spin–orbit coupling on the quasiparticle density of states (QDOS). a The t_{2g} (QDOS) as defined in the text. The main panel displays the region around E_F while illustrating the influence of the spin–orbit coupling on the location of the van-Hove singularity. The inset shows the QDOS in a broader energy window. The Fermi surface is also shown (right inset). **b** Decomposition of the QDOS into contributions from the *xy*, *zx*, *yz* orbitals, at the critical strain at which the Fermi energy coincides with the van-Hove singularity. The inset displays the corresponding Fermi surface.

at the chemical potential. Our experimental results are shown to be in good agreement with a theoretical analysis based on a quasiparticle description starting from the band-structure evaluated under strain but keeping quasiparticle renormalizations independent on strain. This agreement hence provides further support for the limited role of strain on the quasiparticle renormalizations in this material.

RESULTS

NMR experiments under uniaxial strain

To study the Fermi-liquid crossover upon approaching a van-Hove singularity, we performed ^{17}O NMR experiments on Sr_2RuO_4 under in-plane uniaxial stress ε_{aa} in a temperature range 1.5–50 K at applied field strengths $B = 3$ T and 8 T. The magnetic field $\mathbf{B}\|b$ results in NMR intensity from three oxygen sites, labeled here as two in-plane sites O(1), O(1′), and apical site O(2). For the O(1) site the neighboring Ru sites are along *b* direction, parallel to the magnetic field, hence the corresponding Knight shift is labeled $K_{1\|}$ and for O(1′), where the neighboring Ru sites are perpendicular to the magnetic field, the Knight shift is labeled as $K_{1'\perp}$. (The in-plane site geometry is defined in the Supplementary Information.) Correspondingly, the hyperfine couplings are different, leading to distinct NMR absorption frequencies even in absence of strain. Taking into account also the electric quadrupolar coupling of the five $I = 5/2$ ^{17}O transitions, results in 15 total NMR absorption lines. In this work we focus on the NMR shift of the central transitions for the O(1) and O(1′) sites, which are rendered crystallographically inequivalent due to the B_{1g} component of the strain. As such, the strain-dependent quadrupolar effects[25] are subtracted out in the analysis, so as to isolate the hyperfine contribution to the total shift.

The measured shifts are shown in Fig. 1 where strain is seen to have a pronounced effect on the temperature dependence of the normal state behavior, and particularly so for the O(1) site. The applied stress for each measurement is referenced to the critical value ε_v corresponding to the Lifshitz transition. ε_v is determined empirically by tuning through a maximum in the shift magnitude concomitant with the transition[25] (see Methods and Supplementary Information). In the unstrained case (black), an extremum is seen in the data at ~ 40 K followed by a crossover to the *T*-independent shift expected for a FL for temperatures $T < T_{FL} \sim 30$ K[11,31]. T_{FL} thus obtained is consistent with the FL crossover temperature observed by other methods[1]. The crossover temperature is observed to shift to lower value upon application of the **a**-axis stress ($\varepsilon_{aa} = 0.65\varepsilon_v$, red). At the critical strain ($\varepsilon_{aa} = \varepsilon_v$, green), $T_{FL} \to 0$. Additionally, at sufficiently low temperature the magnetic response is distinctly nonlinear at ε_v, shown in the inset of Fig. 1.

Both the strong temperature dependence of the Knight shift under unstrained conditions, and the striking low-temperature variations of the shifts, especially in $K_{1\|}$ while subjected to strain can be interpreted in the band-structure framework in terms of proximity to the van-Hove singularity in the γ band. For strains lower than the critical one, the van-Hove singularity (as shown in Fig. 2) is located at positive energy E_{vHs}. The non-monotonic dependence of the Knight shift emerges due to a thermal depopulation of states as temperature drops below E_{vHs}. Under strained conditions, the Fermi level moves toward the energy at the vHS, which explains both higher values of the Knight shift and the vanishing of the crossover scale.

Theoretical modeling of quasiparticle response

To make this discussion more quantitative, we consider a simple theoretical modeling in terms of quasiparticles. We introduce the quasiparticle Hamiltonian: $\hat{H}_0^{qp} = \sqrt{\hat{Z}}\,\hat{H}_{KS}\,\sqrt{\hat{Z}}$. In this expression, $\hat{H}_{KS}$ is the Hamiltonian of Kohn–Sham states obtained from density-functional theory (DFT) (we use the generalized gradient approximation), and $\hat{Z}$ is a matrix of quasiparticle weights, which reflect the correlation-induced renormalizations relating physical

electrons to low-energy quasiparticles. We construct $\hat{H}_{KS}$ by performing DFT calculations for a set of strains between 0.0% and 0.8%. We apply strain in the ⟨100⟩ direction and scale the ⟨010⟩ and ⟨001⟩ direction according to the experimentally determined Poisson ratios, $-\varepsilon_{yy}/\varepsilon_{xx} = 0.508$ and $-\varepsilon_{zz}/\varepsilon_{xx} = 0.163$[32]. We consider a minimal set of three low-energy bands, construct maximally localized Wannier functions[33,34] of t_{2g} symmetry and express $\hat{H}_{KS}$ in this minimal basis set of localized orbitals. The matrix of quasiparticle weights $\hat{Z}$ is diagonal in this localized basis and we use $Z_{xy} = 0.166$ and $Z_{xz/yz} = 0.275$ for $T \leq 30$ K. These values are the renormalizations found from DMFT calculations in the Fermi-liquid regime of the unstrained material[8], which are consistent with the mass enhancements obtained from ARPES[16], optical spectroscopy[17] and quantum oscillations experiments[35]. We also take into account that, above ~ 30 K, the renormalization is gradually reduced as temperature is increased, using $Z(T)$ obtained in ref. [8].

Spin–orbit coupling (SOC) plays a key role in the physics of Sr_2RuO_4. As in refs. [16,20,21,36,37], we take SOC into account in $\hat{H}_{KS}$ as a local atomic term in the t_{2g} basis. The bare DFT value of the SOC is about 0.1 eV. However, it is established from both theoretical calculations and experiments[16,20,21,36] that electronic correlations lead to an effective enhancement of the SOC to roughly 0.2 eV. The quasiparticle density of states (QDOS) associated with $\hat{H}_0^{qp}$ for unstrained Sr_2RuO_4 for 0.0, 0.1, and 0.2 eV SOC is shown in Fig. 2a. We see that including the (enhanced) SOC moves the vHs closer to the Fermi level. As a consequence, the critical strain corresponding to the Lifshitz transition is strongly reduced, an observation also made in refs. [25,32]. By taking the enhancement of the SOC into account, we find a critical strain $\varepsilon_{aa} \sim -0.5\%$, as shown in Fig. 2b, which is in good agreement with the experimental value of $-0.44 \pm 0.06\%$[32]. We note that by taking only the bare SOC into account, the critical strain is nearly a factor of two too large.

We calculate the magnetic susceptibility $\chi^{qp}(T)$ associated with the non-interacting quasiparticle Hamiltonian $\hat{H}_0^{qp}$ by adding a magnetic field term and placing ourselves in the linear response regime (for details, see Methods). Orbitally resolved results are displayed in Fig. 3, as a function of temperature and for several values of the strain. The *xz*, *yz* component has a weak temperature and strain dependence, corresponding to a featureless shape of the density-of-states for that orbital. In contrast, χ_{xy}^{qp} depends strongly on temperature and strain, due to the proximity to a 2D van-Hove singularity, resembling the behavior observed for the Knight shifts. For all values of the strain except the critical one, χ_{xy}^{qp} displays a temperature-independent (Pauli) plateau at low-*T*. The temperature below which the plateau behavior is found decreases as strain is increased, and vanishes at the critical strain. On warming to temperatures $T > T_{FL}$, the susceptibility first increases, as expected from the fact that a large density of states is thermally accessible close to the vHs, and then decreases on further warming. Secondary to the effect of the vHs, the temperature-dependent quasiparticle renormalization also contributes to the decrease in χ^{qp} above 30 K, as shown explicitly in the Supplementary Information.

It is instructive to place our simple description in the broader context of a Landau theory of the Fermi-liquid state. In such a theory, quasiparticles interact and the magnetic susceptibility (in a simple single-band framework) is given by: $\chi = \chi_0 \frac{m^*/m}{1+F_0^a}$ where m^*/m is the quasiparticle mass renormalization, F_0^a is a Landau interaction parameter and χ_0 is the bare susceptibility in the absence of any renormalizations. Our simple model only takes into account the $\chi_0 \frac{m^*}{m}$ part of this expression (note that within a local description of the Fermi-liquid state $m^*/m = 1/Z$). In other words, we assume that the dominant action is in the change in quasiparticle dispersions (fermiology of the system) as strain is applied, and not in the strain dependence of the Landau

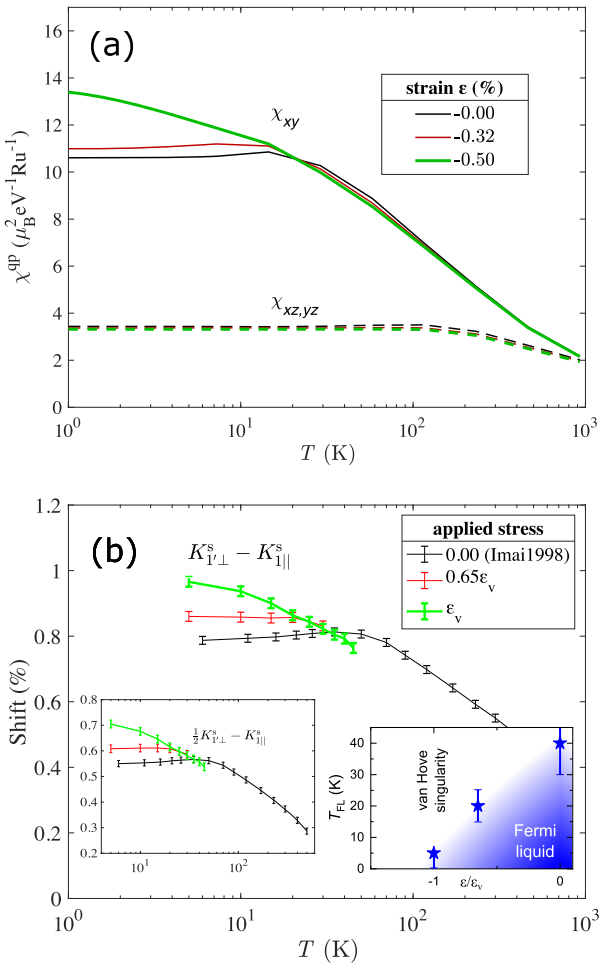

Fig. 3 Comparison between calculated and measured susceptibility. a Susceptibility evaluated from the quasiparticle Hamiltonian as a function of temperature and *a*-axis strain, $\chi^{qp}(\varepsilon_{aa}, T)$. The susceptibility is resolved into contributions from the three t_{2g} orbitals. The critical (compressive) strain is close to $\varepsilon_{aa} = -0.50\%$. **b** Experimentally determined $K^s_{1'\perp} - K^s_{1||}$ as a function of temperature and applied stress, referenced to the critical stress ε_v. K^s denotes the spin part of the total shift. To calculate the difference continuously, shifts have been interpolated from Fig. 1 after subtraction of the known orbital contribution. ($K^o_{1||} = +0.18\%$, $K^o_{1'\perp} = 0.0\%$)[40]. Error bars are determined by the average linewidth of the two sites. The inset on the right illustrates the Fermi-liquid crossover temperature as a function of uniaxial strain, extracted from our Knight-shift data. The defining criterion is the shift extremum separating the regimes of *T*-independent behavior, and that of logarithmic *T*-dependence. Error bars denote the temperature range in which the shift variation about the extremum is less than the linewidth.

interaction parameters, which we assume to be weak. We also neglected the possible strain-dependence of the effective mass enhancements $\hat{Z}$. Our working assumption of strain independent renormalizations is supported by good agreement with the experimental data presented here, but should be further quantified by other means, such as measurements of specific heat[38] or high-resolution angular-resolved photoemission experiments. It should also be addressed by more elaborate computational approaches, such as dynamical mean-field theory, when the methods will allow for reliable solutions in the presence of spin–orbit coupling and low temperatures <10 K—for recent progress in this direction, see refs. [36,39].

DISCUSSION

In order to make a semi-quantitative comparison of the calculations to the experiment it is convenient to take linear combinations of the measured Knight shifts to extract the orbital contributions to the susceptibility[11]. Indeed, the measured ^{17}O Knight shifts in Fig. 1 include contributions from the spin responses associated with each of the three Fermi surfaces, as well as orbital contributions. Previous ^{17}O NMR work[40] determined the orbital shift for the two sites to be $K^{o}_{1||} = +0.18\%$, $K^{o}_{1'\perp} = 0.0\%$; both values are consistent with recent examinations of the superconducting state[41,42]. Subtracting these terms from the total shifts shown in Fig. 1 leaves behind the contributions proportional to the electronic spin response K_s. The remaining ^{17}O shift contributions are known to arise mostly from dipolar coupling to the occupied p-orbitals[11,43]. The tetragonal geometry then implies a coupling to the magnetization of the in-plane p-orbital for the O(1′) site that is twice as large and with opposite sign to that of the O(1), while the couplings to the out-of-plane orbitals dominating the α, β bands are equivalent. As such, subtracting the shifts of both sites, as shown in the main panel of Fig. 3b, eliminates the shared contribution from the $d_{xz/yz}$ bands. Hence this quantity is, to first approximation, proportional to the d_{xy} susceptibility. (The inset removes the factor 2 weighting for the O(1′) shift and is representative of the average over the γ-band states within T of μ. Such a linear combination does not fully eliminate the contribution from xz/yz states, but due to the weak temperature and strain dependence of $\chi_{xz/yz}$ this contribution is just an approximately constant offset).

It should be noted, however, that under strained conditions the in-plane oxygen p_x and p_y orbitals are no longer equivalent, which complicates the analysis. The effects of the asymmetry are amplified by the relative sensitivities of the O(1), O(1′) sites to the singularity at Y. Namely, the momentum-dependent overlap $|b_{\mathbf{k}}|$ of oxygen 2p states with the hybridized γ-band wave functions is far greater for the O(1) site, than for the O(1′) site for momenta near Y[25]. We discuss further this effect in the Supplementary Information.

So, how do the calculated χ_{xy} and the difference between the two oxygen shifts compare? At zero strain (black points), there is good semi-quantitative agreement. At $\varepsilon_{aa} = 0.65\,\varepsilon_v$ (red), and $\varepsilon_{aa} = \varepsilon_v$ (green), the calculated susceptibility has the same qualitative behavior as the measured $K^{s}_{1'\perp} - K^{s}_{1||}$. As strain is increased, the FL coherence temperature is driven to zero $T_{FL} \to 0$ and $E_\gamma(Y) \to 0$ $(\varepsilon \to \varepsilon_v)$. Furthermore, the agreement between the low-temperature strain enhancement of the susceptibility is also reasonable, with about 23% enhancement observed in $K^{s}_{1'\perp} - K^{s}_{1||}$ compared to 17% in the calculated χ^{qp}_{xy} at 4 K. The calculated unstrained FL crossover temperature in Fig. 3a is slightly lower than that seen in the measured shifts (about 20 K, or reduced by half relative to the maximum at 40 K, see the right inset of Fig. 3b, a discrepancy that can be explained by the underestimation of $E_F - E_{vHs} \simeq 7$ meV inherent to the calculation (experiments suggest $E_F - E_{vHs} \simeq 10$–14 meV)[15]. As such, the ability of the quasiparticle framework described in this work to reproduce the salient behavior observed in the measured ^{17}O Knight shifts provides strong support for the interpretation that the Fermi-liquid crossover, as well as the approximately logarithmic T-dependence for $T > T_{FL}$, is a consequence of the close proximity of E_F to a (quasi-)2D singularity in the DOS. Interestingly, judging from the agreement, the quasiparticle renormalizations do not substantially increase under strain, at least in the studied temperature range. For a system at the actual 2D singularity one could expect the mass enhancement to also exhibit a logarithmic growth upon lowering T. Whether this growth simply occurs with a small prefactor and hence quantitatively the effects are small down to 2 K, or, alternatively, other effects such as small but finite warping of the Fermi surfaces in the z direction could also play a role remains to be investigated in future work.

In considering the implications for the superconducting ground state, it is natural to expect that the strain response of T_c might similarly be dominated by the QDOS enhancement. For example, in a BCS weak coupling theory we have $T_c = \omega e^{-1/N_{qp}V}$, with the coupling constant V and N_{qp} the QDOS. Using the results calculated here, $\delta N_{qp}/N_{qp} \simeq 15\%$, leads to $\delta T_c/T_c = 2.5$ (an unusual feature of the present case is that the strongly field-dependent shifts at the critical strain imply that the QDOS varies substantially over the gap scale). Note that, by symmetry, the gap vanishes at Y for any odd parity order parameter, hence the above scenario is consistent with the prior evidence for even parity superconductivity from Knight shift measurements[41,42].

We emphasize that, in order to keep our theoretical description simple, we did not consider two possible effects, which should be addressed in future work. The first is a possible strain-dependence of the quasiparticle mass enhancements, and the second is the strain-dependence of the Stoner enhancement factor $1/(1 + F_0^a)$. However, the striking agreement with experiment found here, neglecting these effects, suggests they are not crucial to understanding the Fermi-liquid behavior near the Lifshitz transition. We note however that an increase of the Stoner factor under strain was found in a previous density-functional theory calculation[25]. Another interesting issue is the departure from Fermi-liquid theory at the critical strain[25,30]. In tetragonal Sr_2RuO_4, the quasiparticle coherence is well-known to be resilient to temperatures exceeding the nominal T_{FL}[6,17,22–24], and we also note that measurements of the temperature-dependent bulk DC susceptibility (detailed in the Supplementary Information) are consistent with that of the NMR shifts even up to 300 K. These observations support the use of a quasiparticle framework to describe the strained material as done here, but a full DMFT calculation performed under strain and at low temperature would be an important check on this approach.

To summarize, the normal state transition from an incoherent-like regime to a Fermi-liquid-like regime in Sr_2RuO_4 is shown tunable by the application of in-plane strain. The crossover temperature is driven to lower values as the critical strain is approached, as shown in the right inset of Fig. 3b, corresponding to the Lifshitz transition for Sr_2RuO_4. Near to the critical strain, the quasiparticle description remains valid, and the increased density of states inferred from the NMR shift enhancements appears qualitatively consistent with the increase in superconducting transition temperature. The results imply that the proximity to the van-Hove singularity is a dominant factor for the macroscopic normal state properties over a broad temperature range. In the unstrained material, this framework naturally accounts for the temperature variation of the susceptibility for $T > T_{FL}$, which was previously not well understood. In spite of the strong effect of the van-Hove singularity on the crossover temperature, which is consistent with what is found in transport[29,32], the effects of the strain on the quasiparticle renormalization are found to be limited. In comparison to earlier work on doped samples or films[15,26] the level of disorder is smaller and the singularity correspondingly sharper: the insensitivity of renormalizations to strain is a surprising result that motivates further development of DMFT methods capable of reaching lower temperatures and with higher energy resolution.

METHODS

Experimental details

An ^{17}O enriched single crystal of Sr_2RuO_4 with dimensions $3.0 \times 0.4 \times 0.2$ mm was mounted onto a piezo-electric variable stress/strain device (www.razorbillinstruments.com/sdm_downloads/cs120-datasheet) such that the applied uniaxial stress was aligned

with the crystallographic **a**-axis. In this device, the rectangular bar is clamped on two ends, such that the strained portion of approximately 1 mm length forms the bridge between the clamps. The subsequently wound inductive coil and resonant tank circuit (10–50 MHz) was configured for top-tuning/matching, such that the stress axis coincides with the coil symmetry axis, and the field orientation $\mathbf{B_0}\|\mathbf{b}$ when placed in the variable temperature cryostat. Compressive stress was applied to the sample in-situ via an external voltage to the piezo-electric stacks of the strain device. The NMR frequencies of the ^{17}O central transitions ($-1/2 \leftrightarrow +1/2$) were measured at applied field strengths $B = 3\text{T}, 8\text{T}$, strains ($\varepsilon_{aa} = 0$, $\varepsilon_{aa} = 0.65\varepsilon_v$, $\varepsilon_{aa} = \varepsilon_v$), and covering temperatures $T = 1.5 - 50$ K. For the O(1′) site there is a discrepancy between the absolute values of the unstrained shift reported in ref. [11] compared to those of refs. [43,25], and the current work. However, the temperature-dependent changes, which are of interest here are consistent throughout. As such, to compare appropriately a constant offset of −0.055% was added to the $K_{1'\perp}$ data of ref. [11] plotted in Fig. 1 and Fig. 3.

Throughout, the strains are referenced to the critical compressive strain at the Lifshitz transition, which was identified empirically by tuning through an extremum in the NMR shifts; these measurements are detailed in the Supplementary Information. The critical strain was estimated in a previous NMR work[25] to be $\varepsilon_{aa} \simeq -0.59\%$, using a capacitive sensor to measure the relative distance changes between the sample clamps in the strain device. The displacements measured by this method overestimate the actual compressive strain, because it does not take into account deformations of the epoxy and the strain device. A corrected value for the critical a-axis strain ($\varepsilon_{aa} = -0.44\%$) was first obtained in ref. [32] by incorporating a force sensor into the device, and taking into account the low-temperature elastic moduli obtained from Resonant Ultrasound Spectroscopy measurements.

Computational details

We use the experimental lattice parameters $a = b = 3.8613$ Å, $c = 12.7218$ Å from ref. [44] measured at 8 K. The internal coordinates (apical O and Sr z-position) of the unstrained structure were relaxed within DFT resulting in $z_O = 0.16344$ and $z_{Sr} = 0.35230$ (compared to the experimental ones of: 0.1634(4) and 0.3529(4)). For simplicity, we do not optimize the internal coordinates under strain. We confirmed with calculations at higher strains that the internal coordinates are not affected much by the applied strain. The DFT calculations have been performed with WIEN2k[45] within the generalized gradient approximation[46], using RKmax = 8 and a shifted $27 \times 27 \times 27$ k-grid.

For the Wannier construction we use wien2wannier[47] and Wannier90[48], a $10 \times 10 \times 10$ k-grid and a frozen energy window ranging from −1.77 to 3 eV for all strains.

For the calculation of the susceptibility we evaluate the up/down spin DOS under an applied magnetic field of 2 T on a very dense $3360 \times 3360 \times 3360$ k-grid and an energy grid with a spacing of 0.28 meV.

Parts of the calculations have been performed using the TRIQS library[49].

DATA AVAILABILITY

Excel data will be deposited in https://www.pa.ucla.edu/content/sr2ruo4-knightshift-vs-temperature.

CODE AVAILABILITY

Code used for the calculations in the main text and Supplementary Information will be deposited in https://www.pa.ucla.edu/content/sr2ruo4-knightshift-vs-temperature.

Received: 13 February 2022; Accepted: 2 November 2022;
Published online: 02 December 2022

REFERENCES

1. Mackenzie, A. P. & Maeno, Y. The superconductivity of Sr_2RuO_4 and the physics of spin-triplet pairing. *Rev. Mod. Phys.* **75**, 657–712 (2003).
2. Georges, A., de' Medici, L. & Mravlje, J. Strong correlations from hund's coupling. *Annu. Rev. Condens. Matter Phys.* **4**, 137–178 (2013).
3. Mackenzie, A. P., Scaffidi, T., Hicks, C. W. & Maeno, Y. Even odder after twenty-three years: the superconducting order parameter puzzle of Sr_2RuO_4. *npj Quant. Mater.* **2**, 40 (2017).
4. Mackenzie, A. P. A personal perspective on the unconventional superconductivity of Sr_2RuO_4. *J. Supercond. Nov. Magn.* **33**, 177–182 (2020).
5. Kivelson, S. A., Yuan, A. C., Ramshaw, B. & Thomale, R. A proposal for reconciling diverse experiments on the superconducting state in Sr_2RuO_4. *npj Quantum Mater.* **5**, 43 (2020).
6. Tyler, A. W., Mackenzie, A. P., NishiZaki, S. & Maeno, Y. High-temperature resistivity of Sr_2RuO_4: Bad metallic transport in a good metal. *Phys. Rev. B* **58**, R10107–R10110 (1998).
7. Mravlje, J. et al. Coherence-incoherence crossover and the mass-renormalization puzzles in Sr_2RuO_4. *Phys. Rev. Lett.* **106**, 096401 (2011).
8. Kugler, F. B. et al. Strongly correlated materials from a numerical renormalization group perspective: How the fermi-liquid state of Sr_2RuO_4 emerges. *Phys. Rev. Lett.* **124**, 016401 (2020).
9. Maeno, Y. et al. Two-dimensional fermi liquid behavior of the superconductor Sr_2RuO_4. *J. Phys. Soc. Jpn.* **66**, 1405–1408 (1997).
10. Maeno, Y. et al. Superconductivity in a layered perovskite without copper. *Nature* **372**, 532–534 (1994).
11. Imai, T., Hunt, A. W., Thurber, K. R. & Chou, F. C. ^{17}o nmr evidence for orbital dependent ferromagnetic correlations in Sr_2RuO_4. *Phys. Rev. Lett.* **81**, 3006–3009 (1998).
12. Bergemann, C., Mackenzie, A. P., Julian, S. R., Forsythe, D. & Ohmichi, E. Quasi-two-dimensional fermi liquid properties of the unconventional superconductor Sr_2RuO_4. *Adv. Phys.* **52**, 639–725 (2003).
13. Mackenzie, A. P. et al. Quantum oscillations in the layered perovskite superconductor Sr_2RuO_4. *Phys. Rev. Lett.* **76**, 3786–3789 (1996).
14. Damascelli, A. et al. Fermi surface, surface states, and surface reconstruction in Sr_2RuO_4. *Phys. Rev. Lett.* **85**, 5194–5197 (2000).
15. Shen, K. M. et al. Evolution of the fermi surface and quasiparticle renormalization through a van hove singularity in $Sr_{2-y}La_yRuO_4$. *Phys. Rev. Lett.* **99**, 187001 (2007).
16. Tamai, A. et al. High-resolution photoemission on Sr_2RuO_4 reveals correlation-enhanced effective spin-orbit coupling and dominantly local self-energies. *Phys. Rev. X* **9**, 021048 (2019).
17. Stricker, D. et al. Optical response of Sr_2RuO_4 reveals universal fermi-liquid scaling and quasiparticles beyond landau theory. *Phys. Rev. Lett.* **113**, 087404 (2014).
18. Haverkort, M. W., Elfimov, I. S., Tjeng, L. H., Sawatzky, G. A. & Damascelli, A. Strong spin-orbit coupling effects on the fermi surface of Sr_2RuO_4 and Sr_2RhO_4. *Phys. Rev. Lett.* **101**, 026406 (2008).
19. Veenstra, C. et al. Spin-orbital entanglement and the breakdown of singlets and triplets in Sr_2RuO_4 revealed by spin- and angle-resolved photoemission spectroscopy. *Phys. Rev. Lett.* **112**, 127002 (2014).
20. Zhang, G., Gorelov, E., Sarvestani, E. & Pavarini, E. Fermi surface of Sr_2RuO_4: spin-orbit and anisotropic coulomb interaction effects. *Phys. Rev. Lett.* **116**, 106402 (2016).
21. Kim, M., Mravlje, J., Ferrero, M., Parcollet, O. & Georges, A. Spin-orbit coupling and electronic correlations in Sr_2RuO_4. *Phys. Rev. Lett.* **120**, 126401 (2018).
22. Shirakawa, N. et al. Novel hall-coefficient behavior in superconducting Sr_2RuO_4. *J. Phys. Soc. Jpn.* **64**, 1072–1075 (1995).
23. Mackenzie, A. P. et al. Hall effect in the two-dimensional metal Sr_2RuO_4. *Phys. Rev. B* **54**, 7425–7429 (1996).
24. Zingl, M., Mravlje, J., Aichhorn, M., Parcollet, O. & Georges, A. Hall coefficient signals orbital differentiation in the hund's metal Sr_2RuO_4. *npj Quantum Mater.* **4**, 35 (2019).
25. Luo, Y. et al. Normal state ^{17}O NMR studies of Sr_2RuO_4 under uniaxial stress. *Phys. Rev. X* **9**, 021044 (2019).
26. Burganov, B. et al. Strain control of fermiology and many-body interactions in two-dimensional ruthenates. *Phys. Rev. Lett.* **116**, 197003 (2016).
27. Barber, M., Gibbs, A., Maeno, Y., Mackenzie, A. & Hicks, C. Resistivity in the vicinity of a van hove singularity: Sr_2RuO_4 under uniaxial pressure. *Phys. Rev. Lett.* **120**, 076602 (2018).
28. Sunko, V. et al. Direct observation of a uniaxial stress-driven lifshitz transition in Sr_2RuO_4. *npj Quant. Mater.* **4**, 46 (2019).

29. Herman, F. c. v., Buhmann, J., Fischer, M. H. & Sigrist, M. Deviation from fermi-liquid transport behavior in the vicinity of a van hove singularity. *Phys. Rev. B* **99**, 184107 (2019).
30. Stangier, V. C., Berg, E. & Schmalian, J. Breakdown of the wiedemann-franz law at the lifshitz point of strained Sr_2RuO_4. *Phys. Rev. B* **105**, 115113 (2022).
31. Nourafkan, R. & Acheche, S. Temperature dependence of the NMR knight shift in pnictides: Proximity to a van hove singularity. *Phys. Rev. B* **98**, 161116 (2018).
32. Barber, M. E. et al. Role of correlations in determining the van hove strain in Sr_2RuO_4. *Phys. Rev. B* **100**, 245139 (2019).
33. Marzari, N. & Vanderbilt, D. Maximally localized generalized wannier functions for composite energy bands. *Phys. Rev. B* **56**, 12847–12865 (1997).
34. Souza, I., Marzari, N. & Vanderbilt, D. Maximally localized wannier functions for entangled energy bands. *Phys. Rev. B* **65**, 035109 (2001).
35. Mackenzie, A. P. et al. The fermi surface topography of Sr_2RuO_4. *J. Phys. Soc. Jpn.* **67**, 385–388 (1998).
36. Linden, N.-O., Zingl, M., Hubig, C., Parcollet, O. & Schollwöck, U. Imaginary-time matrix product state impurity solver in a real material calculation: Spin-orbit coupling in Sr_2RuO_4. *Phys. Rev. B* **101**, 041101 (2020).
37. Karp, J. et al. Sr_2MoO_4 and Sr_2RuO_4: Disentangling the Roles of Hund's and van Hove Physics. *Phys. Rev. Lett.* **125**, 166401 (2020).
38. Li, Y.-S. et al. High-sensitivity heat-capacity measurements on Sr_2RuO_4 under uniaxial pressure. *Proc. Natl Acad. Sci. USA* **118**, e2020492118 (2021).
39. Cao, X., Lu, Y., Hansmann, P. & Haverkort, M. W. Tree tensor-network real-time multiorbital impurity solver: Spin-orbit coupling and correlation functions in Sr_2RuO_4. *Phys. Rev. B* **104**, 115119 (2021).
40. Ishida, K. et al. Spin-triplet superconductivity in Sr_2RuO_4 identified by ^{17}O knight shift. *Nature* **396**, 658–660 (1998).
41. Pustogow, A. et al. Constraints on the superconducting order parameter in Sr_2RuO_4 from oxygen-17 nuclear magnetic resonance. *Nature* **574**, 72–75 (2019).
42. Chronister, A. et al. Evidence for even parity unconventional superconductivity in Sr_2RuO_4. *Proc. Natl Acad. Sci. USA* **118**, e2025313118 (2021).
43. Mukuda, H. et al. Novel character of spin fluctuations in spin-triplet superconductor Sr_2RuO_4:^{17}O-NMR study. *J. Phys. Soc. Jpn.* **67**, 3945–3951 (1998).
44. Vogt, T. & Buttrey, D. J. Low-temperature structural behavior of Sr_2RuO_4. *Phys. Rev. B* **52**, R9843–R9846 (1995).
45. Blaha, P. et al. *WIEN2k, An Augmented Plane Wave + Local Orbitals Program for Calculating Crystal Properties* (Tech. Univ., 2018).
46. Perdew, J. P., Burke, K. & Ernzerhof, M. Generalized gradient approximation made simple. *Phys. Rev. Lett.* **77**, 3865–3868 (1996).
47. Kuneš, J. et al. Wien2wannier: from linearized augmented plane waves to maximally localized wannier functions. *Comput. Phys. Commun.* **181**, 1888–1895 (2010).
48. Mostofi, A. A. et al. wannier90: a tool for obtaining maximally-localised wannier functions. *Comput. Phys. Commun.* **178**, 685–699 (2008).
49. Parcollet, O. et al. TRIQS: a toolbox for research on interacting quantum systems. *Comput. Phys. Commun.* **196**, 398–415 (2015).

ACKNOWLEDGEMENTS

We thank Steve Kivelson and Igor Mazin for helpful discussions. A.P. acknowledges support by the Alexander von Humboldt Foundation through the Feodor Lynen Fellowship. A.C. acknowledges support from the Julian Schwinger Foundation. This work was supported by the National Science Foundation under grant numbers 1709304, 2004553. Work at Los Alamos was supported by the Los Alamos National Laboratory LDRD Program. N.K. is supported by a KAKENHI Grants-in-Aids for Scientific Research (Grant Nos. 17H06136, 18K04715, and 21H01033), and Core-to-Core Program (No. JPJSCCA20170002) from the Japan Society for the Promotion of Science and by a JST-Mirai Program grant (No. JPMJMI18A3). J.M. acknowledges funding by the Slovenian Research Agency (ARRS) under Program No. P1-0044, J1-1696, and J1-2458. The work at Dresden was funded by the Deutsche Forschungsgemeinschaft-TRR 288-422213477 (projects A10 and B01). The Flatiron Institute is a division of the Simons Foundation.

AUTHOR CONTRIBUTIONS

A.C., A.P., Y.L., and S.E.B. designed experiments; A.C., A.P., Y.L., and J.D.T. performed experiments; A.C., A.P., and S.E.B. analyzed data; M.Z., J.M., and A.G. designed computations; M.Z. performed computations; N.K., D.A.S., F.J., and E.D.B. contributed new reagents/analytic tools; N.K. monitored sample growth; D.A.S., F.J., C.W.H., and A.P.M. contributed to sample characterization; E.D.B. contributed to sample alignment, cutting, and oxygenation; and A.C., M.Z., A.P., C.W.H., A.P.M., J.M., A.G., and S.E.B. wrote the manuscript.

COMPETING INTERESTS

The authors declare no competing interests.

ADDITIONAL INFORMATION

Supplementary information The online version contains supplementary material available at https://doi.org/10.1038/s41535-022-00519-6.

Correspondence and requests for materials should be addressed to A. Chronister or S. E. Brown.

Reprints and permission information is available at http://www.nature.com/reprints

Publisher's note Springer Nature remains neutral with regard to jurisdictional claims in published maps and institutional affiliations.